

# Probing initial geometrical anisotropy and final azimuthal anisotropy in heavy-ion collisions at Large Hadron Collider energies through event-shape engineering

Suraj Prasad<sup>1</sup>, Neelkamal Mallick<sup>1</sup>, Sushanta Tripathy<sup>2</sup>, and Raghunath Sahoo<sup>1\*</sup>

<sup>1</sup>*Department of Physics, Indian Institute of Technology Indore, Simrol, Indore 453552, India and*

<sup>2</sup>*INFN - sezione di Bologna, via Irnerio 46, 40126 Bologna BO, Italy*

(Dated: July 26, 2022)

Anisotropic flow is accredited to have effects from the initial state geometry and fluctuations in the nuclear overlap region. The elliptic flow ( $v_2$ ) and triangular flow ( $v_3$ ) coefficients of the final state particles are expected to have influenced by eccentricity ( $\varepsilon_2$ ) and triangularity ( $\varepsilon_3$ ) of the nucleons, respectively. In this work, we study  $v_2$ ,  $v_3$ ,  $\varepsilon_2$ ,  $\varepsilon_3$  and the correlations among them with respect to event topology in the framework of a multi-phase transport model (AMPT). We use transverse sphericity and reduced flow vector as event shape classifiers in this study. Transverse sphericity has the unique ability to separate events based on geometrical shapes, i.e., jetty and isotropic, which pertain to pQCD and non-pQCD domains of particle production in high-energy physics, respectively. We use the two-particle correlation method to study different anisotropic flow coefficients. We confront transverse sphericity with a more widely used event shape classifier – reduced flow vector ( $q_n$ ) and they are found to have significant (anti-)correlations among them. We observe significant sphericity dependence on  $v_2$ ,  $v_3$  and  $\varepsilon_2$ . This work also addresses transverse momentum dependent crossing points between  $v_2$  and  $v_3$ , which varies for different centrality and sphericity percentiles.

PACS numbers:

## I. INTRODUCTION

The goal of ultra-relativistic heavy-ion collisions is to produce a thermalised deconfined medium of quarks and gluons that existed shortly after the Big Bang. These deconfined partons in thermal equilibrium is well known as quark-gluon plasma (QGP). Since QGP can not be detected directly, several indirect signatures have been proposed to signify the formation of a hot and dense medium. Proton-proton (pp) collisions are traditionally used as a baseline to study some of these signatures in heavy-ion collisions. However, recently, some of the heavy-ion-like signatures of QGP have been observed in pp collisions [1–4] which compelled the scientific community to investigate pp collisions from different aspects using state of the art methods. Transverse sphericity is one such observable which separates events based on geometrical shapes, such as jetty and isotropic events. So far, transverse sphericity is broadly explored in pp collisions [5–13]; however, it is still novel for heavy-ion collisions. A recent study [14] of transverse sphericity in heavy-ion collisions shows that many of the global observables in heavy-ion collisions such as kinetic freeze-out temperature, mean transverse radial flow velocity, mean transverse mass, integrated yield, etc., strongly correlate with transverse sphericity.

The anisotropic flow is related to momentum space azimuthal anisotropy and it is parameterised by the coefficients of Fourier expansion of momentum distribution. These anisotropic flow coefficients are closely associated

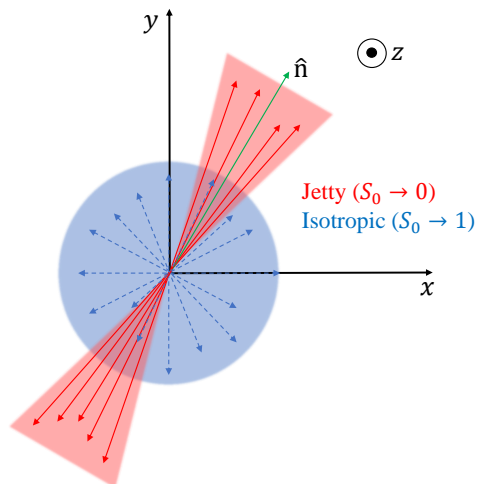


FIG. 1: (Color Online) Schematic picture showing jetty and isotropic events in the transverse plane.

with initial geometry as well as its fluctuations and the equation of state of the medium formed. QGP behaves like a perfect fluid, and anisotropic flow studies at Relativistic Heavy Ion Collider (RHIC) and Large Hadron Collider (LHC) energies show that it has a viscosity to entropy density ratio ( $\eta/s$ ) close to  $1/4\pi$  [15, 16], which is the lower bound as imposed by the quantum mechanical considerations based on supersymmetric gauge theory in infinite coupling limit [17, 18]. With an increase in the order of flow coefficients, their sensitivity to  $\eta/s$  increases, i.e., triangular flow is more sensitive to  $\eta/s$  than elliptic flow [15]. Using flow coefficients, one can infer the flu-

\*Corresponding Author email: Raghunath.Sahoo@cern.ch

idity of the medium formed; for example, a lower value of the second-order flow coefficient, elliptic flow, corresponds to a relatively higher value of  $\eta/s$  and vice versa [15]. The comparison of hydrodynamic studies with the experimentally measured anisotropic flow values shows that the major contribution of the anisotropic flow is expected to arise from the partonic medium and evolve with the evolution of QGP [19–23]. However, this is not all to the anisotropic flow, because it also has effects from the hadronic rescattering [24, 25]. Both these contributions lead to the number of constituent quarks (NCQ) scaling hierarchy of different particles in anisotropic flow at intermediate transverse momentum ( $p_T$ ) range, i.e., baryons have more flow compared to mesons [26]. However, this NCQ scaling on elliptic flow is violated at LHC energies [19, 27]. In recent studies [28, 29], it has been observed that elliptic flow anti-correlates with transverse sphericity [28] i.e., events with higher values of sphericity (isotropic events) have lower elliptic flow and vice versa. This result is expected, since high sphericity events are isotropic in nature, thus its momentum space azimuthal anisotropy is expected to be less. A study on the NCQ scaling of elliptic flow at LHC energies shows that the scaling is violated for the integrated and jetty types of events [29]. So far the sensitivity of transverse sphericity on higher harmonic flow coefficients and initial state geometrical anisotropy are yet to be investigated.

This study aims to address the dependence of transverse sphericity on eccentricity, triangularity, elliptic and triangular flow using a multi-phase transport model (AMPT). We also perform a detailed study on the correlation of transverse sphericity with more traditional event shape observable, i.e, reduced flow vector [30].

This paper is organised as follows. We begin with a brief introduction and motivation of the study in section I. Then we discuss the event generation and analysis methodology in section II, where we introduce AMPT and transverse sphericity. In section III, we define the formulations of eccentricity, triangularity, elliptic flow, and triangular flow and discuss our results. Finally, in section IV, we summarise our results with important findings.

## II. EVENT GENERATION AND ANALYSIS METHODOLOGY

In this section, we briefly discuss the event generator i.e., a multi-phase transport model which is used in this study. Then we discuss and compare the event classifiers used for event topology analysis.

### A. A Multi-Phase Transport (AMPT) Model

AMPT model includes both initial partonic collisions and final hadronic interactions and the transition between these two phases of matter. It has four main

components, namely, initialization of collisions, parton transport after initialization, hadronization mechanism and hadron transport [31–47]. A brief discussion on the main components of AMPT can be found in the appendix section. Since, the particle flow and spectra are well described at mid- $p_T$  region by quark coalescence mechanism for hadronisation [48, 49], we have used AMPT-SM mode (AMPT version 2.26t9b) for our study. The AMPT settings in the current study are the same as reported in Ref. [50]. Centrality selection has been done using impact parameter slicing and we have used the impact parameter values for different centralities from Ref. [51] for our current analysis.

### B. Event shape observables

#### 1. Transverse sphericity ( $S_0$ )

Transverse sphericity ( $S_0$ ) is an event topology classifier that is used to separate events based on geometrical shapes. Transverse sphericity can be defined for a unit vector  $\hat{n}(n_T, 0)$  as follows:

$$S_0 = \frac{\pi^2}{4} \min \left( \frac{\sum_i |p_{T_i} \times \hat{n}|}{\sum_i |p_{T_i}|} \right)^2 \quad (1)$$

where  $p_{T_i}$  denotes transverse momentum of hadron  $i$  and  $i$  runs over all the final state hadrons in an event.  $\hat{n}$  is chosen such that the bracketed term in Eq. 1 is minimised. This selection is done by iterating through all the possible values of  $\hat{n}$  in the transverse plane for the event. Multiplication of  $\pi^2/4$  in Eq. 1 ensures that  $S_0$  is normalised between 0 and 1. The two extreme limits of  $S_0$ , namely, 0 and 1 correspond to the jetty (pencil-like) and isotropic events, respectively. Figure 1 represents a schematic picture showing jetty and isotropic events in the transverse plane. In order to create similar conditions as in ALICE experiment at the LHC, we only select particles with  $|\eta| < 0.8$  and  $p_T > 0.15$  GeV/ $c$  with a minimum constraint of 5 charged particles in a collision. For the sake of simplicity, in this paper, we may sometimes refer transverse sphericity as sphericity. Here we separate events based on sphericity i.e., by choosing extreme 20% events from the sphericity distribution as done in Refs.[14, 28]. We call the events having highest and lowest 20% values in the  $S_0$  values as high- $S_0$  and low- $S_0$  events, respectively. The sphericity cuts for high- $S_0$  and low- $S_0$  events are given in Table I. In a recent study,  $v_2$  is found to be strongly correlated with  $S_0$  [28]. This motivates us to look for the correlations among the sphericity and more traditional event shape classifier in heavy-ion collisions, i.e., the reduced flow vector ( $q_n$ ).

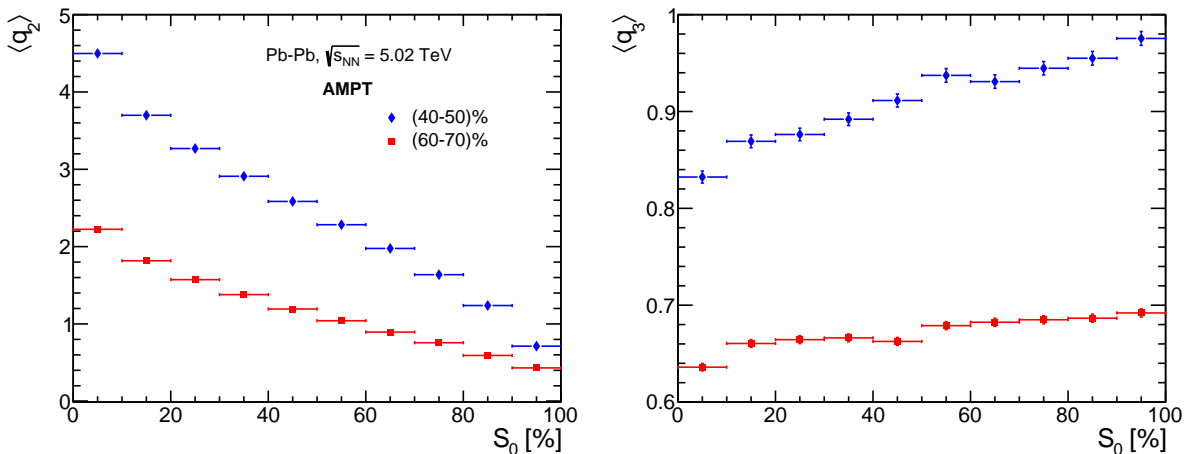


FIG. 2: (Color Online) Event averaged  $q_2$  (left) and  $q_3$  (right) vs transverse sphericity ( $S_0$ ) for mid-central, and peripheral Pb-Pb collisions at  $\sqrt{s_{\text{NN}}} = 5.02$  TeV using AMPT model.

TABLE I: Low- $S_0$  and high- $S_0$  cuts on sphericity distribution for different centrality classes in Pb-Pb collisions at  $\sqrt{s_{\text{NN}}} = 5.02$  TeV [14, 28].

Centrality (%)	Low- $S_0$	High- $S_0$
0-10	0 – 0.880	0.953 – 1
10-20	0 – 0.813	0.914 – 1
20-30	0 – 0.760	0.882 – 1
30-40	0 – 0.735	0.869 – 1
40-50	0 – 0.716	0.865 – 1
50-60	0 – 0.710	0.870 – 1
60-70	0 – 0.707	0.873 – 1

## 2. Reduced flow vector ( $q_n$ )

Another event classifier, called as reduced flow vector ( $q_n$ ) is traditionally used in heavy-ion collisions to perform event shape engineering. The magnitude of reduced flow vector of order- $n$  [30] is given as,

$$q_n = \frac{|Q_n|}{\sqrt{M}} \quad (2)$$

where,

$$Q_n = \sum_{j=1}^M e^{in\phi_j}, \quad (3)$$

$\phi_j$  is the azimuthal angle of  $j^{\text{th}}$  particle at the kinetic freeze-out,  $M$  is the multiplicity of the event, and  $i$  is the imaginary unit number.

In the limit,  $M \rightarrow \infty$ ,  $q_2$  approaches transverse energy ( $E_T$ ) weighted single particle elliptic flow ( $v_2$ ) [52, 53].  $q_n$  are found to be strongly correlated with  $v_n$  values as shown in Ref. [53]. For the sake of comparison of  $q_n$  with

transverse sphericity in the same footing, similar  $\eta$  and  $p_T$  cuts have been applied in  $q_n$  calculations as done in transverse sphericity. The left panel of Fig. 2 represents the correlation between sphericity and  $q_2$ , where both of them are observed to be anti-correlated, i.e., high- $S_0$  events have lower  $q_2$  values and vice versa. However, in the right side plot of Fig. 2, where  $\langle q_3 \rangle$  is shown against different  $S_0$  selections, we observe a mild positive correlation of  $\langle q_3 \rangle$  with  $S_0$ . This correlation between sphericity and  $q_3$ , indicates a finite dependence of  $v_3$  on sphericity [53].

## III. RESULTS AND DISCUSSIONS

In this section, we present a detailed discussion on the sphericity dependence of the geometry of the nuclear overlap region, i.e., eccentricity and triangularity (III A). Then we discuss the methodology and results on coefficients of anisotropic flow and the interplay among them as a function of sphericity, presented in section III B.

### A. Eccentricity and Triangularity

The overlap region in a non-central heavy-ion collision is not isotropic in space. If the pressure gradient of the hot and dense medium formed in the heavy-ion collisions is large enough, the anisotropy in initial geometry can be translated into final momentum space azimuthal anisotropy. The anisotropy in the initial spatial distribution of the nucleons in the overlap region can be quantified by the quantities such as eccentricity ( $\varepsilon_2$ ), triangularity ( $\varepsilon_3$ ) etc. As the name suggests, eccentricity refers to how elliptical the medium can be, and is generated due to anisotropy in the nuclear overlap region. Similarly, triangularity characterises the triangular geometry of the overlap region during the collision of two

heavy-ions and arises due to event-by-event fluctuations in the participant nucleon collision points [54]. In the current study, we have used AMPT model to see the dependence of transverse sphericity on eccentricity ( $\varepsilon_2$ ) and triangularity ( $\varepsilon_3$ ) having followed the notations used in Ref. [55]. Eccentricity and triangularity of the participant nuclei can be generalised as follows [55]:

$$\varepsilon_n = \frac{\sqrt{\langle r^n \cos(n\phi_{\text{part}}) \rangle^2 + \langle r^n \sin(n\phi_{\text{part}}) \rangle^2}}{\langle r^n \rangle} \quad (4)$$

where  $r$  and  $\phi_{\text{part}}$  are the polar co-ordinates of the participant nucleons.  $n = 2$  corresponds to eccentricity and  $n = 3$  corresponds to triangularity. A higher value of  $n$  can be used to study higher-order spatial anisotropy of the collision overlap region, although the contributions from the higher order terms will be smaller. In Eq. 4, angular brackets, “ $\langle \dots \rangle$ ” represents the mean taken over all the participant nucleons in an event.

Figure 3 shows the event-average eccentricity ( $\langle \varepsilon_2 \rangle$ ) (top) and triangularity ( $\langle \varepsilon_3 \rangle$ ) (middle) and their ratio (bottom) as a function of centrality for different sphericity events. Both  $\langle \varepsilon_2 \rangle$  and  $\langle \varepsilon_3 \rangle$  have clear dependence on the centrality and are increasing from central to peripheral collisions. This behavior is expected since in central collisions, the nuclear overlap region is more spatially symmetric compared to that in peripheral collisions, resulting in low values of  $\langle \varepsilon_2 \rangle$  and  $\langle \varepsilon_3 \rangle$  in central collisions. However, as one moves towards peripheral collisions, the participating nucleon overlap region gets more and more spatially anisotropic resulting in higher values of  $\langle \varepsilon_2 \rangle$  and  $\langle \varepsilon_3 \rangle$ . In a particular centrality, one notices lower  $\langle \varepsilon_2 \rangle$  for high- $S_0$  events than the low- $S_0$  events. This indicates that transverse sphericity can also be used to distinguish events based on the initial geometry. However, since the contribution in  $\varepsilon_n$  for  $n > 2$  arises due to fluctuations in the density profile of the participating nucleons, one should not expect significant transverse sphericity dependence, as shown in the middle plot of Fig. 3. The bottom plot of Fig. 3 represents the ratio of ( $\langle \varepsilon_3 \rangle$ ) to ( $\langle \varepsilon_2 \rangle$ ), plotted against different centrality classes for high- $S_0$ ,  $S_0$  integrated and low- $S_0$  classes. From the ratio, it is clear that  $\langle \varepsilon_2 \rangle$  is higher than  $\langle \varepsilon_3 \rangle$  for low- $S_0$ , and  $S_0$  integrated events throughout all centrality classes except the most central case where,  $\langle \varepsilon_3 \rangle$  seems to be higher. But the order is reversed for high- $S_0$  events where  $\langle \varepsilon_3 \rangle$  is always greater than  $\langle \varepsilon_2 \rangle$ , indicating the dominance of density fluctuations over the geometry of the overlap region.

## B. Elliptic and Triangular Flow

Anisotropic flow is a measure of the azimuthal momentum anisotropy of the final state particles produced in a collision. Anisotropic flow depends upon initial spatial anisotropy in the nuclear overlap region, transport properties, and the equation of state of the system. Anisotropic flow can be characterised by the coefficients

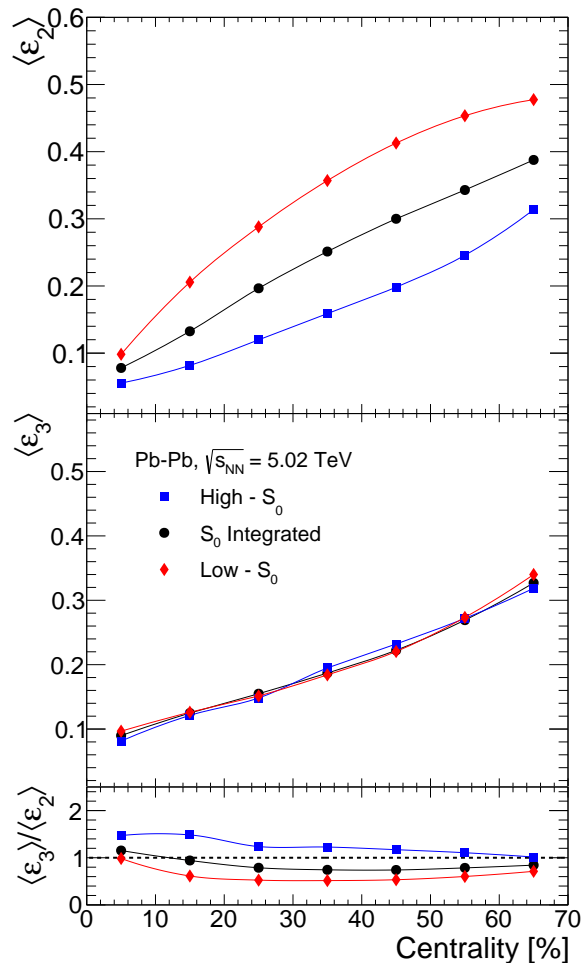


FIG. 3: (Color Online) Event-average eccentricity ( $\langle \varepsilon_2 \rangle$ ) (top), triangularity ( $\langle \varepsilon_3 \rangle$ ) (middle) and the ratio ( $\langle \varepsilon_3 \rangle / \langle \varepsilon_2 \rangle$ ) (bottom) as a function of centrality for low- $S_0$  (red diamond), high- $S_0$  (blue square) and integrated  $S_0$  (black circle) events in Pb-Pb collisions at  $\sqrt{s_{\text{NN}}} = 5.02$  TeV using AMPT.

of the Fourier expansion of momentum distribution of the final state particles and is given by:

$$E \frac{d^3 N}{dp^3} = \frac{d^2 N}{2\pi p_T dp_T dy} \left( 1 + 2 \sum_{n=1}^{\infty} v_n \cos[n(\phi - \psi_n)] \right) \quad (5)$$

Here  $\phi$  is the azimuthal angle of the particles in the transverse plane and  $\psi_n$  is the  $n$ th harmonic event plane angle [19].  $n$  stands for the order of the anisotropic flow coefficient.  $n=2$  stands for elliptic flow ( $v_2$ ) and  $n=3$  refers to the triangular flow ( $v_3$ ). In general  $n$ th order anisotropic flow,  $v_n$  can be defined as:

$$v_n = \langle \cos[n(\phi - \psi_n)] \rangle \quad (6)$$

We are dealing with different kinds of sphericity events and among them, low- $S_0$  events are prone to have contributions from jets. Thus, in order to see the fair depen-

dence of transverse sphericity, we use the two-particle correlation method to study the elliptic and triangular flow as done in Refs. [53, 56, 57]. The two-particle correlation method has an advantage because it deals with the non-flow effects caused by jets and resonance decays by implementing a proper pseudorapidity cut. It has an additional advantage since it does not require event plane angle ( $\psi_n$ ) to calculate  $v_n$ . In experiments, a pseudorapidity dependence of  $\psi_n$  is observed, which is not taken into consideration in the present study for simplicity, which doesn't affect the performed studies. Here we assume  $\psi_n$  to be the global phase angle for all the particles irrespective of the selection of the bins in pseudorapidity [28, 58, 59]. Although in AMPT we can set the reaction plane angle,  $\psi_R = 0$ , this is not trivial in experiments to determine the same. Thus, one follows a two-particle correlation approach. The steps to find the correlation function is as follows:

- We compose two sets of particles based on particle transverse momentum denoted by labels 'a' and 'b'.
- Each particle from 'a' pairs with every particle in 'b' and the relative pseudorapidities ( $\Delta\eta = \eta_a - \eta_b$ ) and the relative azimuthal angles ( $\Delta\phi = \phi_a - \phi_b$ ) are then determined.
- Two particle correlation function ( $C(\Delta\eta, \Delta\phi)$ ) can be constructing by taking the ratio of the same-event pair ( $S(\Delta\eta, \Delta\phi)$ ) distribution to the mixed-event pair distribution ( $B(\Delta\eta, \Delta\phi)$ ). The ratio improves the pair acceptance and ensures no non-uniformity.

In the mixed event background, five events are randomly chosen so that it contains no physical correlation [28]. To remove the non-flow contributions and to obtain 1D correlation in  $\Delta\phi$  distribution, one uses the  $\Delta\eta$  cut in  $S(\Delta\eta, \Delta\phi)$  and  $B(\Delta\eta, \Delta\phi)$  as  $2 \leq |\Delta\eta| \leq 5$  to get  $S(\Delta\phi)$  and  $B(\Delta\phi)$ , respectively. The ratio of  $S(\Delta\phi)$  to  $B(\Delta\phi)$  is given by  $C(\Delta\phi)$ , known as 1D correlation in  $\Delta\phi$  distribution. 1D correlation in  $\Delta\phi$  distribution can also be written as [53, 57]:

$$C(\Delta\phi) = \frac{dN_{\text{pairs}}}{d\Delta\phi} = A \times \frac{S(\Delta\phi)}{B(\Delta\phi)} = A \times \frac{\int S(\Delta\eta, \Delta\phi) d\Delta\eta}{\int B(\Delta\eta, \Delta\phi) d\Delta\eta}, \quad (7)$$

where  $A$  is the normalisation constant given as  $N_{\text{pairs}}^{\text{mixed}}/N_{\text{pairs}}^{\text{same}}$ . Here  $N_{\text{pairs}}^{\text{mixed}}$  and  $N_{\text{pairs}}^{\text{same}}$  are mixed event pairs and same event pairs, respectively in the chosen  $\Delta\eta$  region. The normalisation scaling in Eq. 7 ensures the same number of pairs in mixed-event (B) and same-event (S). The distribution of pairs or 1D correlation function in  $\Delta\phi$  can be Fourier expanded as follows:

$$C(\Delta\phi) = \frac{dN_{\text{pairs}}}{d\Delta\phi} \propto [1 + 2 \sum_{n=1}^{\infty} v_{n,n}(p_T^a, p_T^b) \cos n\Delta\phi] \quad (8)$$

where  $v_{n,n}$  are the two-particle flow coefficients being

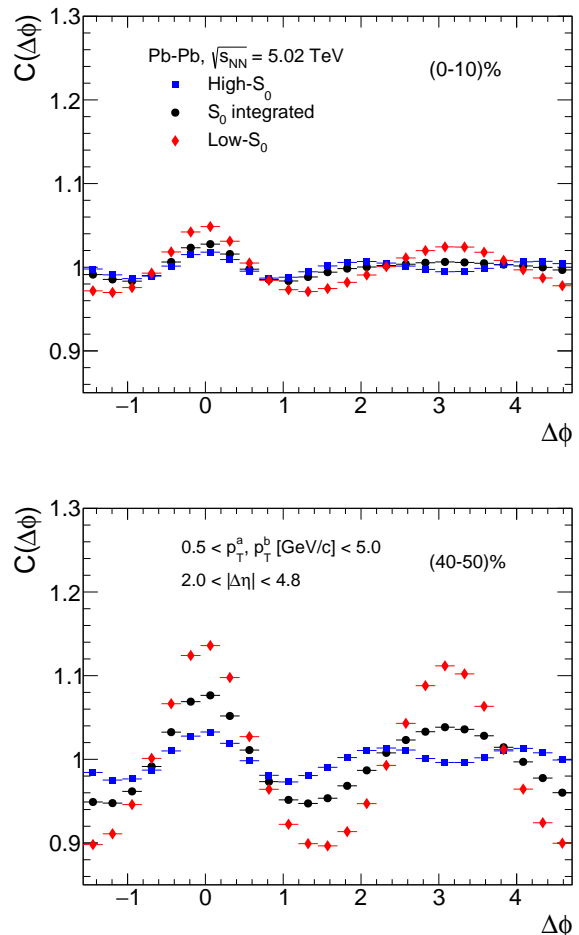


FIG. 4: (Color Online) One dimensional two-particle azimuthal correlation function for low- $S_0$ , high- $S_0$  and  $S_0$  integrated events in Pb-Pb collisions at  $\sqrt{s_{\text{NN}}} = 5.02$  TeV for (0-10)% (top) and (40-50)% (bottom) centrality classes [28].

symmetric with respect to  $p_T^a$  and  $p_T^b$ .  $v_{n,n}$  can be calculated by discrete Fourier transformation as:

$$v_{n,n}(p_T^a, p_T^b) = \langle \cos n\Delta\phi \rangle = \frac{\sum_{m=1}^N \cos(n\Delta\phi_m) C(\Delta\phi_m)}{\sum_{m=1}^N C(\Delta\phi_m)} \quad (9)$$

where  $N$  ( $=200$ ) is the number of bins in the range  $-\pi/2 < \Delta\phi < 3\pi/2$  of  $\Delta\phi$  distribution.

Flow coefficients defined in Eq. 5 contributes to Eq. 8 as:

$$C(\Delta\phi) \propto [1 + 2 \sum_{n=1}^{\infty} v_n(p_T^a) v_n(p_T^b) \cos n\Delta\phi] \quad (10)$$

In Eq. 10, the event plane angle drops out during the convolution leaving only the dependence on an azimuthal angle. If one assumes that the collective flow is driven by azimuthal anisotropy, then the two-particle harmonic co-

efficient ( $v_{n,n}$ ) should be a product of two single-particle harmonic coefficients. Therefore,

$$v_{n,n}(p_T^a, p_T^b) = v_n(p_T^a)v_n(p_T^b) \quad (11)$$

Another way around, we can calculate  $v_n$  from  $v_{n,n}$  by using the following expression

$$v_n(p_T^a) = \frac{v_{n,n}(p_T^a, p_T^b)}{\sqrt{v_{n,n}(p_T^b, p_T^b)}} \quad (12)$$

A crucial point to note here that, negative value of  $v_{n,n}(p_T^b, p_T^b)$  in Eq. 12 makes  $v_n(p_T^a)$  imaginary which is not physical. The correlation function and the anisotropic flow coefficients such as elliptic and triangular flow are calculated in the pseudorapidity range  $|\eta| < 2.5$ , and a relative pseudorapidity gap of  $2 < |\Delta\eta| < 4.8$  in the transverse momentum range of the particle pairs from 0.5 to 5 GeV/c [28]. Figure 4 shows the transverse sphericity dependence on one dimensional two-particle azimuthal correlation function plotted with respect to  $\Delta\phi$  for (0-10)% and (40-50)% centralities in Pb-Pb collisions at  $\sqrt{s_{NN}} = 5.02$  TeV. The larger correlation for mid-central collisions compared to the central collisions indicates more azimuthal anisotropy in mid-central than the central collisions. There is a strong dependence of the correlation function on the sphericity for any particular centrality. One can infer from Fig. 4 that low- $S_0$  events have more azimuthal anisotropy than high- $S_0$  events. Two peaks in the away side in  $\Delta\phi$  for high- $S_0$  events manifest due to higher contribution from  $v_3$ .

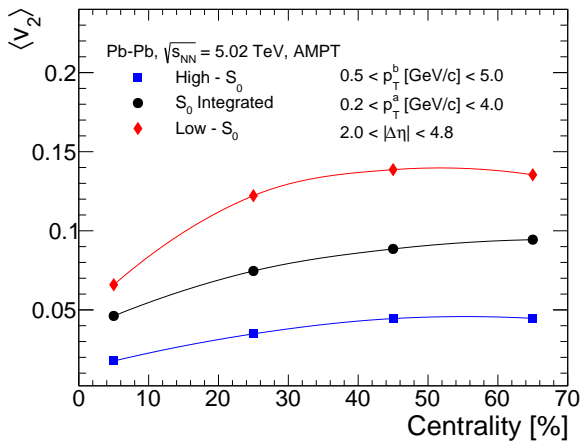


FIG. 5: (Color Online) Mean elliptic flow ( $\langle v_2 \rangle$ ) vs centrality for different sphericity classes in Pb-Pb collisions at  $\sqrt{s_{NN}} = 5.02$  TeV.

Figure 5 represents centrality dependence of elliptic flow ( $\langle v_2 \rangle$ ) for different sphericity classes in Pb-Pb collisions at  $\sqrt{s_{NN}} = 5.02$  TeV. In high-energy heavy-ion collisions, due to the presence of a pressure gradient formed

in the medium, anisotropy in the geometry of the initial nuclear overlap region is transformed into final state azimuthal anisotropy. Since central collisions are almost isotropic in geometry, corresponding  $v_2$  is also less. However, if one moves towards mid-central collisions, the elliptic flow coefficient increases since the eccentricity are higher. However, in peripheral collisions, although eccentricity is remarkably high, due to the lack of the number of participants and low-pressure gradient, spatial anisotropy can not be completely transformed into  $v_2$ . Figure 5 also shows that the value of elliptic flow significantly depends on event selection-based transverse sphericity. Low- $S_0$  events have higher  $\langle v_2 \rangle$  while we observe almost negligible  $\langle v_2 \rangle$  in high- $S_0$  events.

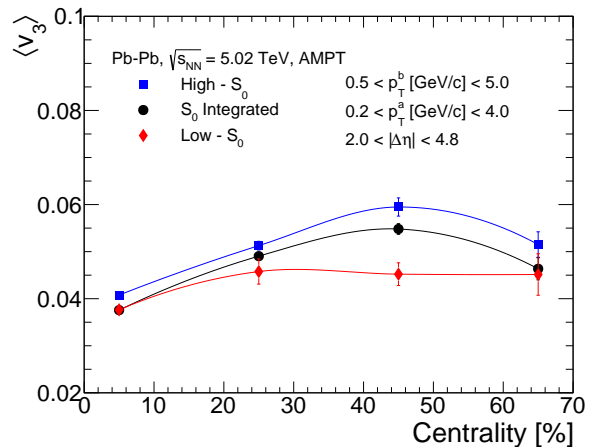


FIG. 6: (Color Online) Mean triangular flow ( $\langle v_3 \rangle$ ) as a function of centrality for different sphericity classes in Pb-Pb collisions at  $\sqrt{s_{NN}} = 5.02$  TeV.

Figure 6 shows triangular flow ( $\langle v_3 \rangle$ ) as a function of centrality for different sphericity classes. In mid-central collisions, one observes slightly higher  $v_3$  than the central collisions for a specific sphericity class. The dependence of  $v_3$  on centrality is weaker than that of  $v_2$ , which can also be observed from Figs. 5 and 6. This weak dependence of  $v_3$  on centrality is also observed in experiments [53, 60]. In addition, one can observe appreciable dependence of triangular flow on transverse sphericity. In Fig. 5,  $v_2$  contribution is maximum in case of low- $S_0$  events while in Fig. 6 the trend is reversed and high- $S_0$  events have dominating  $v_3$ . This anti-correlation between  $v_2 - v_3$  for  $q_2$ -selection as pointed out in Ref. [53] can also be deduced from this study with transverse sphericity. However the anti-correlation between  $\varepsilon_2 - \varepsilon_3$  is not observed in Fig. 3. One may infer that the source of this anti-correlation between  $v_2 - v_3$  with sphericity selection may not be propagated from the initial geometry but may have effects from the medium during its evolution due to the fact that the fluidity of the medium affects differently to different flow coefficients. This is an indication that

the fluidity of the medium is sphericity-dependent. In Ref. [61], authors have shown the dependence of specific shear viscosity ( $\eta/s$ ) on the correlation between triangularity and triangular flow, where the correlation decreases with an increase in  $\eta/s$  and the correlation between  $v_3$  and  $\varepsilon_3$  is not strong in an ideal or minimally viscous fluid. Only (65-70)% of the triangular flow is related to initial triangularity, conveying that a substantial part of the triangular flow is unrelated to the initial triangularity. This may be the reason for the observed dependence of triangular flow on transverse sphericity, while triangularity of the overlap region does not have any sphericity dependence.

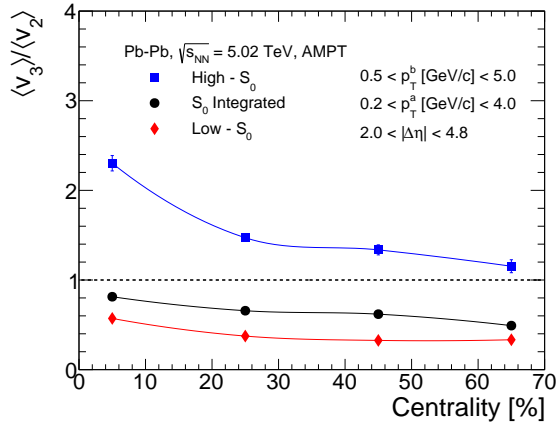


FIG. 7: (Color Online) Ratio  $\langle v_3 \rangle / \langle v_2 \rangle$  vs centrality for different sphericity events in Pb-Pb collisions at  $\sqrt{s_{NN}} = 5.02$  TeV.

Figure 7 represents the ratio  $\langle v_3 \rangle / \langle v_2 \rangle$  versus centrality for different sphericity events. One notices that  $\langle v_3 \rangle / \langle v_2 \rangle$  is decreasing when going from central to peripheral collisions and shows considerable sphericity dependence. This may be because of three reasons; due to the reminiscent centrality dependence of  $\langle \varepsilon_3 \rangle / \langle \varepsilon_2 \rangle$  and/or due to viscous effects [60], or have a contribution from both the effects. One observes  $\langle \varepsilon_3 \rangle / \langle \varepsilon_2 \rangle$  vs centrality trend is followed by  $\langle v_3 \rangle / \langle v_2 \rangle$  starting from most central until semi central collisions. Here, with small changes in centrality, the viscous effect might cause a little change in  $\langle v_3 \rangle / \langle v_2 \rangle$ , however, for the peripheral collisions, the viscous effects play a major role and  $\langle \varepsilon_3 \rangle / \langle \varepsilon_2 \rangle$  trend is not followed by  $\langle v_3 \rangle / \langle v_2 \rangle$  for all sphericity classes. One can notice that  $\langle v_3 \rangle / \langle v_2 \rangle$  is highest and always greater than one for high- $S_0$  events showing the dominance of  $v_3$  over  $v_2$  for all centrality classes and the low- $S_0$  curve shows the dominance of  $v_2$  over  $v_3$ . This effect is expected to have propagated from initial geometry, which is evident from  $\langle \varepsilon_3 \rangle / \langle \varepsilon_2 \rangle$  plot shown in Fig. 3.

Figure 8 represents the elliptic and triangular flow normalised with eccentricity and triangularity, respectively, as a function of centrality in Pb-Pb collisions at  $\sqrt{s_{NN}}$

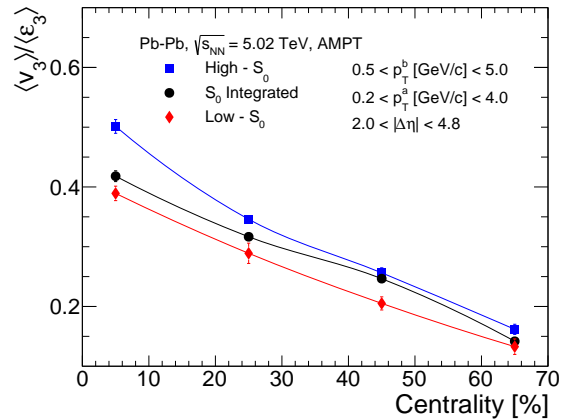
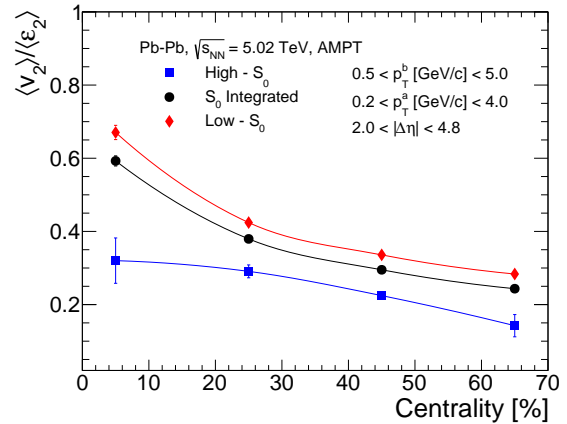


FIG. 8: (Color Online)  $\langle v_2 \rangle / \langle \varepsilon_2 \rangle$  (top) and  $\langle v_3 \rangle / \langle \varepsilon_3 \rangle$  (bottom) vs centrality for different sphericity classes in Pb-Pb collisions at  $\sqrt{s_{NN}} = 5.02$  TeV using AMPT.

= 5.02 TeV using AMPT. The figure qualitatively tells about the response of the medium formed, and its evolution to different centrality and sphericity selections. In a perfect fluid,  $v_n \propto \varepsilon_n$  and thus  $v_n / \varepsilon_n$  is expected to be a constant value. However, in Fig. 8, both  $\langle v_2 \rangle / \langle \varepsilon_2 \rangle$  and  $\langle v_3 \rangle / \langle \varepsilon_3 \rangle$  are found to be varying with sphericity and centrality. As we move from central to peripheral collisions,  $\langle v_n \rangle / \langle \varepsilon_n \rangle$  decreases. This trend with respect to different centrality selection is also observed in experimental results [60].

Figure 9 shows single particle triangular flow ( $v_3(p_T^a)$ ) as a function of  $p_T$  for different centrality classes for (40-50)% centrality in Pb-Pb collisions at  $\sqrt{s_{NN}} = 5.02$  TeV.  $v_3(p_T^a)$  shows an increase with  $p_T$  from low to intermediate  $p_T$  region, attains a maximum, and starts decreasing towards higher  $p_T$ . Similar trend is observed in Ref. [28] for  $v_{2,2}(p_T^a, p_T^b)$  and  $v_2(p_T^a)$ . One observes a remarkable dependence of transverse sphericity on the triangular flow when compared to elliptic flow. High- $S_0$  events have the highest  $v_3(p_T^a)$  value, whereas low- $S_0$  events have the least  $v_3(p_T^a)$  value.

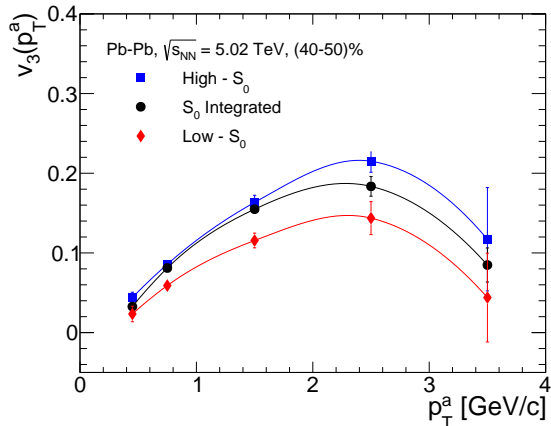


FIG. 9: (Color Online) Single particle triangular flow ( $v_3(p_T^a)$ ) for high- $S_0$ ,  $S_0$  integrated and low- $S_0$  events for Pb-Pb collisions at  $\sqrt{s_{NN}} = 5.02$  TeV for (40-50)% centrality class.

Figure 10 shows the comparison between elliptic and triangular flow as a function of  $p_T$  for (0-10)% and (40-50)% centrality for different sphericity classes. For the mid-central collisions,  $v_2$  is higher than  $v_3$  except for the high- $S_0$  case. However, in the most central case we observe the domination of  $v_3$  over  $v_2$  after a certain  $p_T$  value. The crossing point in  $p_T$  ( $p_T^{\text{cross}}$ ), where the values of  $v_2$  and  $v_3$  become equal, appear to change for different centrality classes. This behaviour is also observed and is in agreement with experimental data [60, 62, 63], where  $p_T^{\text{cross}}$  is found to be increasing with particles' mass and centrality. As pointed out in Refs. [62, 63], the crossing point between the flow coefficients is attributed to the interplay of these flow coefficients with the radial flow [63]. This is because, for central collisions, the contribution of fluctuations in the initial nuclear distribution is more than the influence of the overlap region on the development of the anisotropic flow. However, in the peripheral collisions, the collision geometry contributes higher than initial density fluctuations [62]. In this work, we go a step ahead and try to see the dependence of  $p_T^{\text{cross}}$  with event topology which is shown explicitly in Fig. 11.  $p_T^{\text{cross}}$  for different centrality and sphericity classes is extracted by fitting a polynomial function to the plots in Fig. 10.  $p_T^{\text{cross}}$  is found to be almost flat for high- $S_0$  events but it is observed to be increasing with centrality for  $S_0$  integrated and low- $S_0$  cases. The expected low  $p_T^{\text{cross}}$  for high- $S_0$  events can be accounted for due to a higher contribution from the initial density fluctuations than the influence of initial collision geometry on the anisotropic flow as shown in Fig. 3.

## IV. SUMMARY

In this paper, we have explored the eccentricity, triangularity, elliptic flow, and triangular flow along with their correlations in Pb-Pb collisions at  $\sqrt{s_{NN}} = 5.02$  TeV in the framework of a multi-phase transport model using event shape engineering tools such as the transverse sphericity. The important findings are summarised below:

- After its successful implementation in small collision systems, in this work, we found a significant correlation of transverse sphericity with the more widely used event shape classifier, the reduced flow vector. This highlights the advantage of using sphericity as a unique event shape classifier across all collision systems at the LHC.
- Since the eccentricity is found to be varying with sphericity selection, elliptic flow is found to be strongly (anti-)correlated with sphericity selection as well. However, triangular flow, unlike triangularity, has a significant dependence on transverse sphericity.
- We report an increase in  $\langle v_3 \rangle / \langle v_2 \rangle$  towards central collisions, and the ratio is always greater than one for high- $S_0$  events. This is expected to be propagated from the initial geometry of the participant nucleons and may have contributions from the medium formed.
- We report a crossing point between  $v_2$  and  $v_3$  at a certain transverse momentum value ( $p_T^{\text{cross}}$ ) which is found to be varying with centrality and transverse sphericity.  $p_T^{\text{cross}}$  is found to be decreasing when going towards central and high- $S_0$  events.

The observables related to the geometry of the nuclear overlap region and the anisotropic flow coefficients are found to be correlated among themselves as well as with transverse sphericity. The anisotropic flow coefficients are expected to have contributed from the medium formed in heavy-ion collisions.

## Appendix

### A. Components of AMPT model

1. Initialization of collisions: This step in AMPT model is performed using HLJING [43], where a differential cross-section of the produced mini-jets in pp collisions are calculated, and produced partons calculated in pp collisions are converted into A-A and p-A collisions by incorporating parameterised shadowing function and nuclear overlap function using inbuilt Glauber Model.

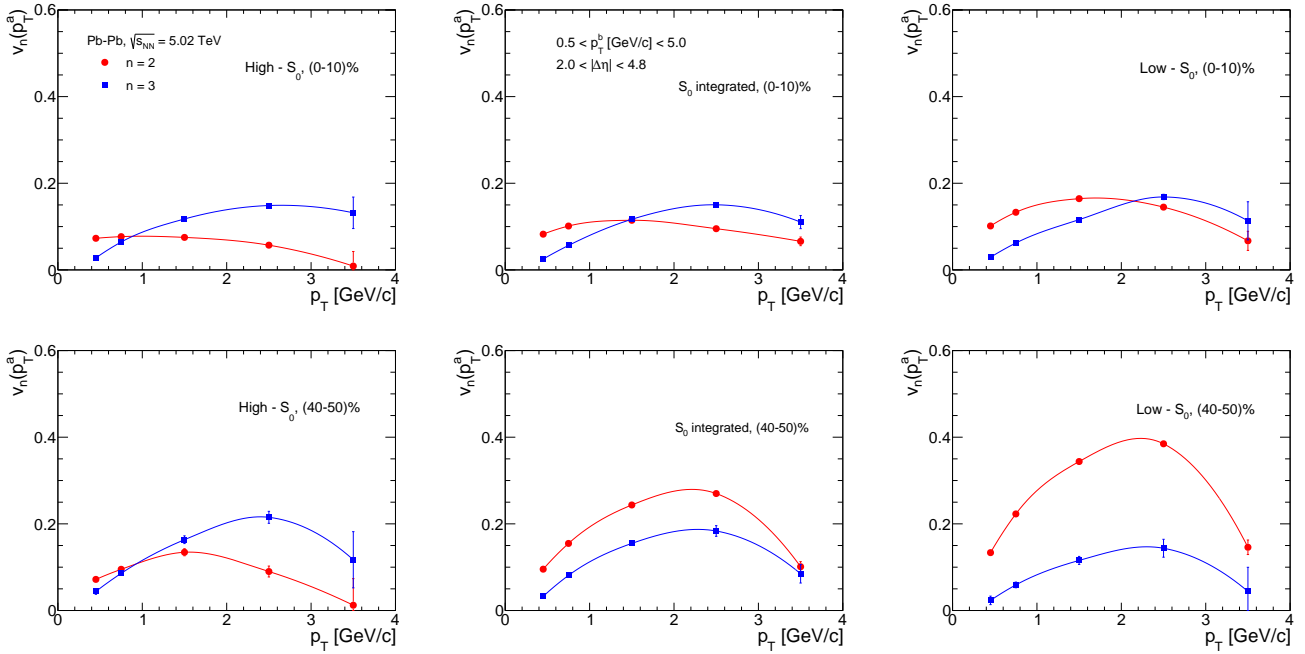


FIG. 10: (Color Online) Single particle elliptic (red) and triangular (blue) flow for high- $S_0$  (left column),  $S_0$  integrated (middle column) and low- $S_0$  (right column) events for Pb–Pb collisions at  $\sqrt{s_{NN}} = 5.02$  TeV for (0-10)% (top) and (40-50)% (bottom) centrality classes using AMPT.

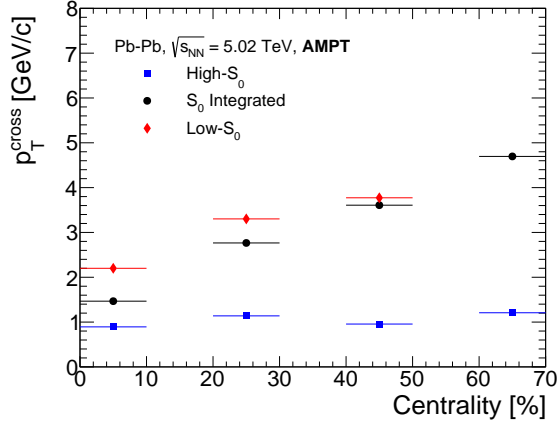


FIG. 11: (Color Online) Transverse momentum value corresponding to crossing between  $v_2$  and  $v_3$  ( $p_T^{\text{cross}}$ ) as a function of centrality for different sphericity cuts for Pb–Pb collisions at  $\sqrt{s_{NN}} = 5.02$  TeV using AMPT.

2. Parton transport: Transportation of produced particles is done using Zhang’s Parton Cascade (ZPC) model [44]. In the String Melting version of AMPT (AMPT-SM), colored strings melt into low-momentum partons.
3. Hadronization: In AMPT-SM, transported partons

are hadronised using spatial coalescence mechanism [37, 45]. In the default AMPT version, a fragmentation mechanism using Lund fragmentation parameters is used to hadronize the transported partons.

4. Hadron transport: The produced hadrons undergo final evolution in relativistic transport mechanism through meson-meson, meson-baryon, and baryon-baryon interactions [46, 47].

## B. Comparison of results from AMPT model and experimental data

Figure 12 shows the comparison of  $\langle v_2 \rangle$  and  $\langle v_3 \rangle$  vs centrality for  $S_0$ -integrated events for Pb–Pb collisions at  $\sqrt{s_{NN}} = 5.02$  TeV using AMPT with ALICE [64] (top) and ATLAS [65] (bottom) results. AMPT is found to be slightly underestimating the elliptic flow from ALICE and ATLAS, however, overestimated the triangular flow. This disagreement between AMPT and experimental data can be fixed using different settings available in AMPT, which is out of the scope of this paper.

## Acknowledgements

SP acknowledges the financial support from UGC, the Government of India. ST acknowledges the support

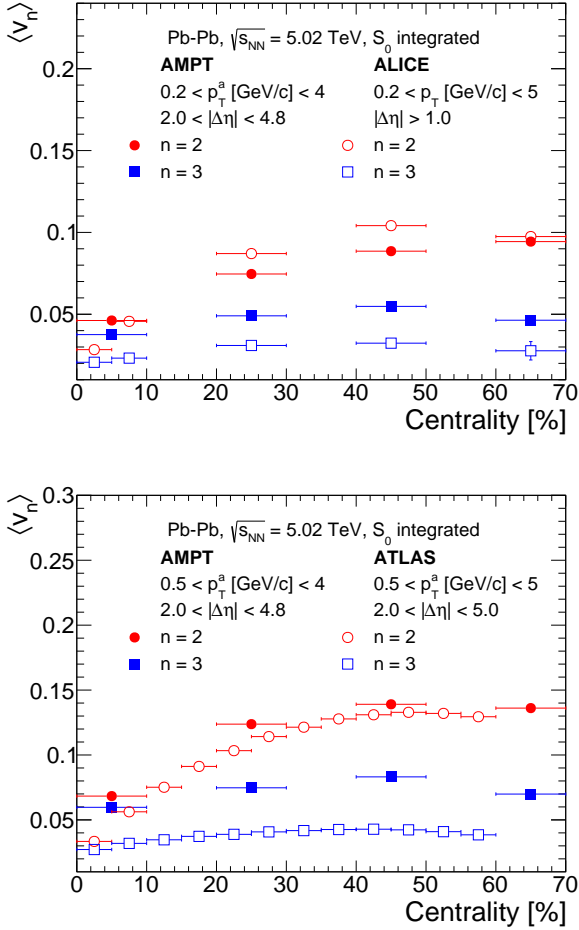


FIG. 12: (Color Online)  $\langle v_2 \rangle$  and  $\langle v_3 \rangle$  vs centrality for  $S_0$  integrated events for Pb–Pb collisions at  $\sqrt{s_{NN}} = 5.02$  TeV using AMPT compared with the similar ALICE [64] (top) and ATLAS [65] (bottom) results.

under the INFN postdoctoral fellowship. RS acknowledges the financial support under DAE-BRNS Project No. 58/14/29/2019-BRNS of the Government of India. The authors would like to acknowledge the usage of resources of the LHC grid Tier-3 computing facility at IIT Indore under the mega-science project grant of DAE-DST, Govt. of India – “Indian participation in the ALICE experiment at CERN” bearing Project No. SR/MF/PS-02/2021-IITI (E-37123).

- 
- [1] J. Adam *et al.* [ALICE Collaboration], *Nature Phys.* **13**, 535 (2017).
- [2] A. Khuntia, H. Sharma, S. Kumar Tiwari, R. Sahoo and J. Cleymans, *Eur. Phys. J. A* **55**, 3 (2019).
- [3] V. Khachatryan *et al.* [CMS Collaboration], *Phys. Lett. B* **765**, 193 (2017).
- [4] J. D. Bjorken, S. J. Brodsky and A. Scharff Goldhaber, *Phys. Lett. B* **726**, 344 (2013).
- [5] E. Cuautle, R. Jimenez, I. Maldonado, A. Ortiz, G. Paic and E. Perez, arXiv:1404.2372 [hep-ph].
- [6] A. Ortiz, G. Paic and E. Cuautle, *Nucl. Phys. A* **941**, 78 (2015).
- [7] G. P. Salam, *Eur. Phys. J. C* **67**, 637 (2010).
- [8] G. Bencédi [ALICE Collaboration], *Nucl. Phys. A* **982**, 507 (2019).
- [9] A. Banfi, G. P. Salam and G. Zanderighi, *JHEP* **1006**, 038 (2010).
- [10] S. Tripathy, A. Bisht, R. Sahoo, A. Khuntia and M. P. Salvan, *Adv. High Energy Phys.* **2021**, 8822524 (2021).
- [11] A. Khuntia, S. Tripathy, A. Bisht and R. Sahoo, *J. Phys. G* **48**, 035102 (2021).
- [12] S. Deb, S. Tripathy, G. Sarwar, R. Sahoo and J. e. Alam, *Eur. Phys. J. A* **56**, 252 (2020).
- [13] A. Khatun, D. Thakur, S. Deb and R. Sahoo, *J. Phys. G* **47**, 055110 (2020).
- [14] S. Prasad, N. Mallick, D. Behera, R. Sahoo and S. Tripathy, *Sci. Rep.* **12**, 3917 (2022).
- [15] B. Schenke, S. Jeon and C. Gale, *Phys. Rev. C* **85**, 024901 (2012).
- [16] C. Gale, S. Jeon, B. Schenke, P. Tribedy and R. Venugopalan, *Phys. Rev. Lett.* **110**, 012302 (2013).
- [17] P. Danielewicz and M. Gyulassy, *Phys. Rev. D* **31**, 53 (1985).
- [18] P. Kovtun, D. T. Son and A. O. Starinets, *Phys. Rev. Lett.* **94**, 111601 (2005).
- [19] B. B. Abelev *et al.* [ALICE Collaboration], *JHEP* **06**, 190 (2015).

- [20] I. Arsene *et al.* [BRAHMS Collaboration], Nucl. Phys. A **757**, 1 (2005).
- [21] C. Shen and U. Heinz, Nucl. Phys. News **25**, 6 (2015).
- [22] B. B. Back *et al.* [PHOBOS Collaboration], Nucl. Phys. A **757**, 28 (2005).
- [23] J. Adams *et al.* [STAR Collaboration], Nucl. Phys. A **757**, 102 (2005).
- [24] T. Hirano, U. W. Heinz, D. Kharzeev, R. Lacey and Y. Nara, Phys. Lett. B **636**, 299 (2006).
- [25] G. S. Pradhan, R. Rath, R. Scaria and R. Sahoo, Phys. Rev. C **105**, 054905 (2022).
- [26] S. A. Voloshin, Nucl. Phys. A **715**, 379 (2003).
- [27] K. Aamodt *et al.* [ALICE Collaboration], Phys. Rev. Lett. **105**, 252302 (2010).
- [28] N. Mallick, R. Sahoo, S. Tripathy and A. Ortiz, J. Phys. G **48**, 045104 (2021).
- [29] N. Mallick, S. Tripathy and R. Sahoo, Eur. Phys. J. C **82**, 524 (2022).
- [30] C. Adler *et al.* [STAR Collaboration], Phys. Rev. C **66**, 034904 (2002).
- [31] B. Zhang, C. M. Ko, B. A. Li and Z. W. Lin, [arXiv:nucl-th/9904075 [nucl-th]].
- [32] B. Zhang, C. M. Ko, B. A. Li and Z. W. Lin, Phys. Rev. C **61**, 067901 (2000).
- [33] B. Zhang, C. M. Ko, B. A. Li, Z. W. Lin and B. H. Sa, Phys. Rev. C **62**, 054905 (2000).
- [34] Z. W. Lin, S. Pal, C. M. Ko, B. A. Li and B. Zhang, Phys. Rev. C **64**, 011902 (2001).
- [35] Z. W. Lin, S. Pal, C. M. Ko, B. A. Li and B. Zhang, Nucl. Phys. A **698**, 375 (2002).
- [36] S. Pal, C. M. Ko and Z. W. Lin, Nucl. Phys. A **730**, 143 (2004).
- [37] Z. W. Lin and C. M. Ko, Phys. Rev. C **65**, 034904 (2002).
- [38] B. Zhang, C. M. Ko, B. A. Li, Z. W. Lin and S. Pal, Phys. Rev. C **65**, 054909 (2002).
- [39] S. Pal, C. M. Ko and Z. W. Lin, Nucl. Phys. A **707**, 525 (2002).
- [40] Z. W. Lin, C. M. Ko and S. Pal, Phys. Rev. Lett. **89**, 152301 (2002).
- [41] Z. W. Lin and C. M. Ko, Phys. Rev. C **68**, 054904 (2003).
- [42] Z. W. Lin and C. M. Ko, J. Phys. G **30**, S263 (2004).
- [43] X. N. Wang and M. Gyulassy, Phys. Rev. D **44**, 3501 (1991).
- [44] B. Zhang, Comput. Phys. Commun. **109**, 193 (1998).
- [45] Y. He and Z. W. Lin, Phys. Rev. C **96**, 014910 (2017).
- [46] B. Li, A. T. Sustich, B. Zhang and C. M. Ko, Int. J. Mod. Phys. E **10**, 267 (2001).
- [47] V. Greco, C. M. Ko and P. Levai, Phys. Rev. C **68**, 034904 (2003).
- [48] R. J. Fries, B. Muller, C. Nonaka and S. A. Bass, Phys. Rev. Lett. **90**, 202303 (2003).
- [49] R. J. Fries, B. Muller, C. Nonaka and S. A. Bass, Phys. Rev. C **68**, 044902 (2003).
- [50] S. Tripathy, S. De, M. Younus and R. Sahoo, Phys. Rev. C **98**, 064904 (2018).
- [51] C. Loizides, J. Kamin and D. d'Enterria, Phys. Rev. C **97**, 054910 (2018) [erratum: Phys. Rev. C **99**, 019901 (2019)].
- [52] J. Schukraft, A. Timmins and S. A. Voloshin, Phys. Lett. B **719**, 394 (2013).
- [53] G. Aad *et al.* [ATLAS Collaboration], Phys. Rev. C **92**, 034903 (2015).
- [54] B. Alver and G. Roland, Phys. Rev. C **81**, 054905 (2010) [erratum: Phys. Rev. C **82**, 039903 (2010)].
- [55] H. Petersen, G. Y. Qin, S. A. Bass and B. Muller, Phys. Rev. C **82**, 041901 (2010).
- [56] A. Adare *et al.* [PHENIX Collaboration], Phys. Rev. C **78**, 014901 (2008).
- [57] G. Aad *et al.* [ATLAS Collaboration], Phys. Rev. C **86**, 014907 (2012).
- [58] V. Khachatryan *et al.* [CMS Collaboration], Phys. Rev. C **92**, 034911 (2015).
- [59] M. Aaboud *et al.* [ATLAS Collaboration], Eur. Phys. J. C **78**, 142 (2018).
- [60] K. Aamodt *et al.* [ALICE Collaboration], Phys. Rev. Lett. **107**, 032301 (2011).
- [61] A. K. Chaudhuri, Phys. Lett. B **713**, 91 (2012).
- [62] J. Adam *et al.* [ALICE Collaboration], JHEP **09**, 164 (2016).
- [63] S. Acharya *et al.* [ALICE Collaboration], JHEP **09**, 006 (2018).
- [64] J. Adam *et al.* [ALICE Collaboration], Phys. Rev. Lett. **116**, 132302 (2016).
- [65] G. Aad *et al.* [ATLAS Collaboration], Phys. Rev. C **101**, 024906 (2020).